DOI: 10.48011/asba.v2i1.1325

Direct-Torque-Control Fault-Tolerant Strategies for Three Induction Motor Drive Systems Operating Under Single-Phase Open-Circuit Fault

Pedro H. M. Martins * **Victor F. M. B. Melo** **
Gilielson F. da Paz *** **Isaac S. de Freitas** ****

* *Federal University of Paraiba (UFPB), PB, Brazil, (e-mail: pedro.martins@cear.ufpb.br).*
** *UFPB, (e-mail: victor@cear.ufpb.br)*
*** *UFPB (e-mail: gilielson@cear.ufpb.br).*
**** *UFPB (e-mail: freitas.isaac@gmail.com).*

Abstract: This paper discusses Direct-torque-control(DTC)-based fault-tolerance strategies applied to three fault-tolerant induction motor drive systems when they operate under single-phase open-circuit fault. Despite the fact that these drive systems have already been discussed in the literature, the reported papers always make use of Field-oriented-control(FOC)-based fault compensation strategies. In this way, performed simulations show that DTC-based strategies are feasible and are able to provide circular flux trajectory, which is the necessary condition for the motor operate properly.

Keywords: DTC, FOC, fault-tolerance, three-phase induction motor drives.

1. INTRODUCTION

In the mid 1980s, Takahashi and Noguchi (1986) proposed a new control method for induction motor named direct torque control (DTC). Based on the reference and estimated values of torque and stator flux, it is possible to directly control the inverter in order to reduce the torque and flux errors, trying to keep the error values within prefixed hysteresis band limits. Thus, the control action, which consists in selecting the appropriate switching state, must be taken in order to minimize flux and torque errors (Casadei et al., 2002).

In this way, DTC scheme is characterized by the absence of current PI regulators, coordinate transformations and PWM signals. In comparison to Field Oriented Control (FOC), these features make DTC much simpler and with lower computational burden. Other advantage of DTC (compared to FOC) is a better performance in transient operating conditions. However, the main disadvantages of DTC are higher current ripple and variable switching frequency (Casadei et al., 2002).

On the other hand, several types of faults may take place in a drive system, one of them being the single-phase open-circuit fault. In this case, one of the motor phases is disconnected from the inverter. The cause may be internal or external to the motor. In order to keep circular flux trajectory after the fault (necessary condition for the motor operate properly), fault-tolerant inverters and strategies must be employed. Welchko et al. (2004) provide a survey on fault-tolerant inverter topologies and strategies proposed in literature, but all of the reported papers make use of FOC-based compensation strategies. Also, Welchko et al. (2004) show that the compensation strategies to be applied in fault occurrences make use of system hardware reconfiguration performed by means of triacs. The three most common fault-tolerant systems, especially for single-phase open-circuit faults, are illustrated in Fig. 1 and are the ones studied in the present paper.

Later on, Dan Sun and Yikang He (2005) and Abassi et al. (2017) discussed a DTC-based fault-tolerant strategy for permanent magnet (PM) drives employing the inverter illustrated in Fig. 1(c). And more recently Scarcella et al. (2017) presented a deadbeat-DTC-based fault-tolerant strategy for PM drives that make use of inverter shown in Fig. 1(a). The deadbeat approach, however, brings much more complexity to the control system and, consequently, a higher computational burden. On the other hand, to these authors' knowledge, DTC-based fault-tolerant strategies have not yet been discussed in the literature for induction motor (IM) drives.

In this context, this paper discusses DTC-based fault-tolerance strategies applied to the three most common fault-tolerant IM drives. Despite the fact that the studied configurations were already discussed in the literature, the employed control techniques were either FOC or open-loop Volts-Hertz control. By means of computer simulations, the feasibility of DTC-based fault tolerant strategies will be proven for all three configurations. Furthermore, these strategies dynamic performance will be compared to FOC-based ones.

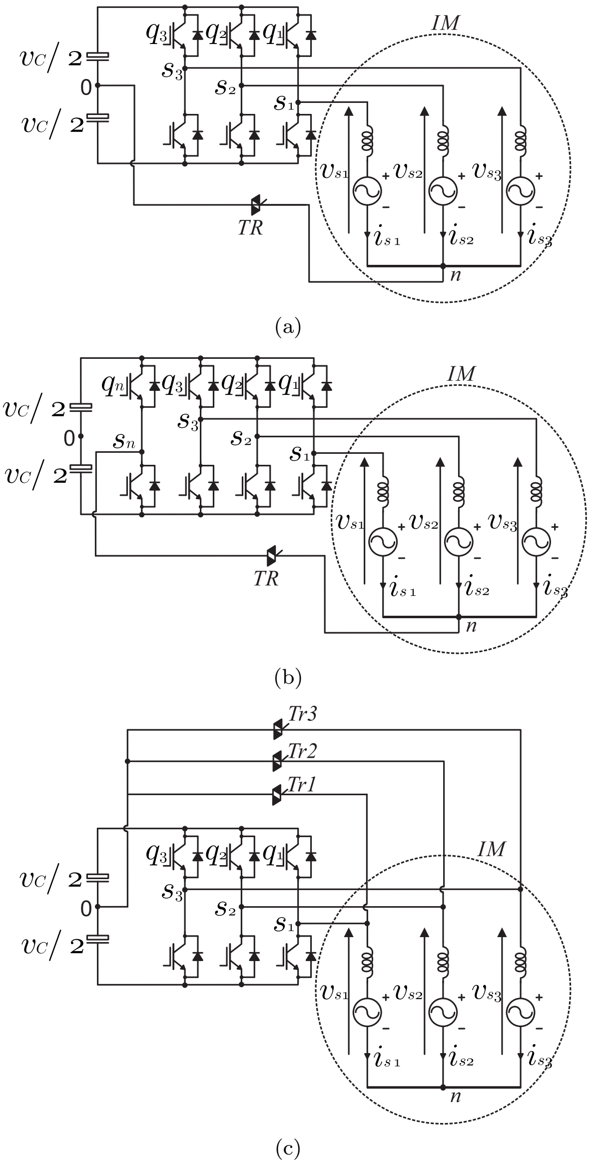

Figure 1. Fault-tolerant drive systems. (a) Configuration 1. (b) Configuration 2. (c) Configuration 3.

2. FAULT-TOLERANT INVERTERS

Configuration 1, illustrated in Fig. 1(a), consists in a three-leg inverter connected to the stator winding of a three-phase squirrel-cage induction motor (IM). The neutral point n of the stator winding is connected to the dc-link mid-point 0 by means of triac TR. During healthy operation TR is always turned-off. In the occurrence of an open-phase fault, TR is activated as part of the compensation strategy, making a zero-sequence current component circulate in the circuit.

Configuration 2, illustrated in Fig. 1(b), is very similar to configuration 1, but neutral point n is connected to a fourth leg s_n by means of triac TR. Naturally, during healthy operation TR is always turned-off. In the occurrence of an open-phase fault, TR is activated as part of the compensation strategy, allowing the circulation of zero-sequence current component. Note that configuration 2 does not require access to the dc-link mid-point, which represents an advantage from the practical point of view. Both configurations 1 and 2 were discussed in (Beltrao de Rossiter Correa et al., 2001) for fault-tolerant operation in three-phase motor drives, but, as mentioned before, applying FOC technique.

At last, configuration 3, shown in Fig. 1(c), connects the three phases to the dc-link mid-point by means of triacs. During healthy condition, these triacs are always turned-off. But if an open-phase fault occurs in any phase due to failure in the respective inverter leg, the triac is activated and connects the affected phase to dc-link mid-point. In this case, there is no zero-sequence current after the fault because the motor operates in a balanced mode similar to healthy operation. This configuration was discussed in (de Araujo Ribeiro et al., 2004), in which the fault-tolerant operation employs open-loop Volts-Hertz control. It is worth pointing out that this configuration has a major disadvantage when compared to the other two, which is the fact that it needs twice the dc-link voltage of healthy operation in order to make the fault compensation strategy operate properly.

3. MACHINE MODEL UNDER FAULT CONDITION

It is known that the machine three-phase variables may be transformed into a two-dimensional domain, usually named dq, and a single-dimensional domain, usually named o as follows

$$f_{s\ dqo} = P_s^T f_{s\ 123}, \tag{1}$$

where $f_{s\ 123} = [f_{s1}\ \ f_{s2}\ \ f_{s3}]^T$ is the machine primary variables matrix and $f_{s\ dqo} = [f_{sd}\ f_{sq}\ f_{so}]^T$ is the machine dq model variables matrix. These variables may be stator voltages ($f = v$) or stator currents ($f = i$). Matrix P_s is obtained considering the stationary common reference frame and is given by

$$P_s = \sqrt{\frac{2}{3}} \begin{bmatrix} 1 & 0 & \frac{1}{\sqrt{2}} \\ \frac{-1}{2} & \frac{\sqrt{3}}{2} & \frac{1}{\sqrt{2}} \\ \frac{-1}{2} & \frac{-\sqrt{3}}{2} & \frac{1}{\sqrt{2}} \end{bmatrix}. \tag{2}$$

The machine stator equations under healthy condition in dq model are

$$v_{sd} = r_s i_{sd} + l_s \frac{di_{sd}}{dt} + l_{sr} \frac{di_{rd}}{dt} \tag{3}$$

$$v_{sq} = r_s i_{sq} + l_s \frac{di_{sq}}{dt} + l_{sr} \frac{di_{rq}}{dt} \tag{4}$$

$$v_{so} = r_s i_{so} + l_{ls} \frac{di_{so}}{dt} \tag{5}$$

and the machine rotor equations are

$$0 = r_r i_{rd} + l_{sr} \frac{di_{sd}}{dt} + l_r \frac{di_{rd}}{dt} + (l_{sr} i_{sq} + l_r i_{rq})\omega_r \tag{6}$$

$$0 = r_r i_{rq} + l_{sr} \frac{di_{sq}}{dt} + l_r \frac{di_{rq}}{dt} - (l_{sr} i_{sd} + l_r i_{rd})\omega_r \tag{7}$$

where r_s and r_r are the stator and rotor windings resistance, respectively, l_s and l_r are the equivalent self-inductance of the stator and rotor windings, respectively, l_{sr} is the stator-rotor equivalent mutual inductance and l_{ls}

is the leakage inductance. i_{rd} and i_{rq} are the rotor direct and quadrature currents, respectively, and ω_r is the rotor electrical frequency in rad/s.

From (1), it is possible to obtain that

$$i_{s1} = \sqrt{\frac{2}{3}}\left(i_{sd} + \frac{1}{\sqrt{2}}i_{so}\right) \tag{8}$$

Now, consider that an open-circuit fault occurs in phase 1, which means $i_{s1} = 0$. In this way, a boundary condition is imposed as

$$i_{so} = -\sqrt{2}i_{sd}. \tag{9}$$

Replacing (9) in (5)

$$v_{so} = -\sqrt{2}r_s i_{sd} - \sqrt{2}l_{ls}\frac{di_{sd}}{dt}. \tag{10}$$

In this way, considering (1) once again and using (3) and (10)

$$v_{s1} = \sqrt{\frac{2}{3}}\left(v_{sd} + \frac{1}{\sqrt{2}}v_{so}\right) = \sqrt{\frac{2}{3}}\left[(l_s - l_{ls})\frac{di_{sd}}{dt} + l_{sr}\frac{di_{rd}}{dt}\right] \tag{11}$$

In this way, in order to digitally simulate the system under an open-circuit fault in machine phase 1, voltage across its terminals (v_{s1}) must be imposed as calculated in (11). By making this, phase 1 current (i_{s1}) assumes null value. In computer simulations, i_{sd} and i_{rd} derivatives present in (11) can be easily calculated using the machine equations and by making

$$\frac{di_{sd}}{dt} = \frac{i_{sd}(k) - i_{sd}(k-1)}{h} \tag{12}$$

$$\frac{di_{rd}}{dt} = \frac{i_{rd}(k) - i_{rd}(k-1)}{h} \tag{13}$$

where k represents the present numerical iteration and $k-1$ represents the previous numerical iteration and h is the simulation time step.

4. HEALTHY DTC AND FAULT-TOLERANT DTC

The control system block diagram for DTC can be seen in (Casadei et al., 2002). In short, the reference value of the stator flux λ_s^* is compared to the estimated value λ_s in order to define the value of variable $d\lambda_s$. On the other hand, a conventional Proportional-Integral (PI) rotor speed controller defines the value of machine reference electromagnetic torque τ_e^*. This value is compared to the estimated value τ_e, defining the value of variable $d\tau_e$. Based on $d\lambda_s$ and $d\tau_e$, and on the position of the stator flux, control action is chosen from a pre-elaborated switching table. Flux and torque are estimated from the measured stator voltages and currents (Casadei et al., 2002).

In this way, hysteresis band limits ($H\lambda$ for flux and $H\tau$ for torque) determine if flux and torque values must increase or decrease. Variables $d\lambda_s$ and $d\tau_e$ assume values -1, 0 or 1 such that:

- if $\tau_e > \tau_e^* + H\tau$, $d\tau_e = -1$, meaning that τ_e must decrease;
- else if $\tau_e < \tau_e^* - H\tau$, $d\tau_e = 1$, meaning that τ_e must increase;
- else if $\tau_e > \tau_e^* - H\tau$ and $\tau_e < \tau_e^* + H\tau$, $d\tau_e = 0$, meaning that τ_e should remain constant.

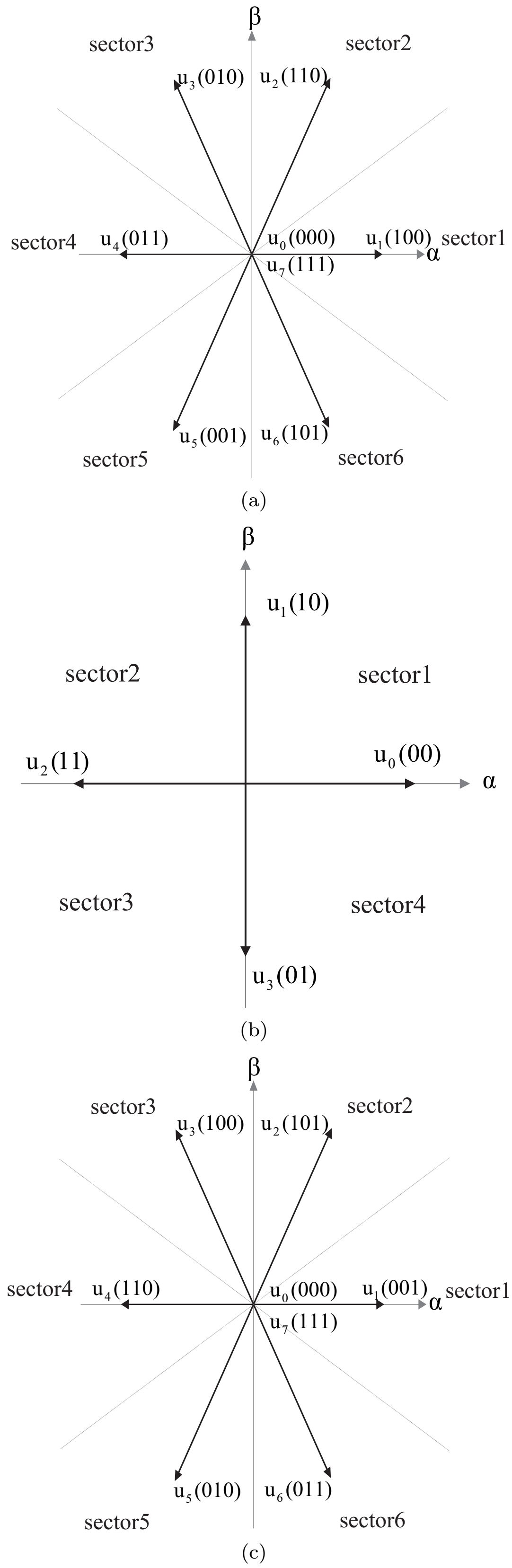

Figure 2. Switching vectors. (a) Healthy operation. (b) Faulty operation - configurations 1 and 3. (c) Faulty operation - configuration 2.

And for flux:

- if $\lambda_s > \lambda_s^* + H\lambda$, $d\lambda_s = 0$, meaning that λ_s must decrease;
- else if $\lambda_s < \lambda_s^* - H\lambda$, $d\lambda_s = 1$, meaning that λ_s must increase.

As explained before, a control action must be taken in order to keep flux and torque values under the hysteresis band limits. This control action consists in selecting the best switching state in order to achieve this goal. For healthy operation, the available switching states are all possible combinations of gating signals q_1, q_2, q_3 (see Fig. 1). The number of these combinations is $2^3 = 8$, being from $[q_1, q_2, q_3]$=[000] to [111], where 0 represents that the leg upper switch is open and 1 represents the leg upper switch is closed.

Also, as discussed in (Casadei et al., 2002; Buja and Kazmierkowski, 2004), the switching states may be mapped, by means of coordinates transformation, in a two-dimensional plane using (1), usually named $\alpha - \beta$ plane. This map may be divided in six sectors for healthy operation. In this way, one may elaborate a switching table with the switching states that must be applied for each condition of $d\tau_e$, $d\lambda_s$ and taking into account the sector in which the stator rotating flux is located. The switching table for this condition is shown in Table 1 and the switching vectors and the sectors are shown in Fig 2(a). The method to elaborate this table is well-known in the literature (Takahashi and Noguchi, 1986). In Table 1, S consists in the number of the sector in which the rotating flux may be located.

However, for configuration 1, consider that an open-circuit fault takes place in phase 1. It means that the gating signal q_1 is no longer part of the switching state since phase 1 is disconnected from the inverter. Note that, in this case, current in phase 1, i_{s1}, becomes null. Also, the available switching states are now composed of all combinations of q_2, q_3, being a total of $2^2 = 4$ possible combinations from $[q_2, q_3]$=[00] to [11]. In this case, $\alpha - \beta$ plane may be divided in four sectors shown in Fig. 2(b) , and a switching table may be elaborated (following the same method used to elaborate Table 1). This table is shown in Table 2.

On the other hand, for configuration 2, considering once again an open-circuit fault in phase 1, gating signal q_n is now added to the switching state combination since leg s_n is now connected to neutral point n. In this way, the available switching states are all possible combinations of q_2, q_3, q_n, from $[q_2, q_3, q_n]$=000 to [111]. In this case, the $\alpha - \beta$ plane may be divided in six sectors shown in Fig. 2(c) and the elaborated switching table is Table 3.

At last, for configuration 3, for an open-circuit fault in phase 1, this phase is connected to the dc-link mid-point. In this way, the switching states are composed of all combinations of q_2, q_3. The elaborated switching table is identical to that of configuration 1, which is Table 2.

5. SIMULATION RESULTS

Simulations were performed for a three-phase 500-W squirrel-cage induction motor. Reference rotor speed was of 360 rad/s and, for DTC, hysteresis limits were $H\lambda =$ 0.002 and $H\tau = 0.02$. A mechanical torque of 1 Nm was imposed. As aforementioned, the proper operation consists in having a circular flux trajectory, which is obtained when the dq currents have same amplitude and are 90° out-of-phase. The induction motor parameters are shown in Table 4. The speed controller gains for both DTC and FOC were $k_{P\omega} = 0.0337$ and $k_{I\omega} = 0.4717$ and the sampling frequency was of 10 kHz. For FOC, the current controller gains were $k_{Pi} = 56.5$ and $k_{Ii} = 39273$ and the triangular carrier compared to reference voltages in order to determine the gating signals was of 10 kHz. For configurations 1 and 2, dc-link voltage was of 684.2 V. For configuration 3, dc-link voltage was of 1185.1 V. As mentioned before, the main disadvantage of configuration 3 is the need of high dc-link voltage for the fault compensation strategy operate properly.

Table 1. Healthy operation DTC switching table.

$d\lambda_s$	$d\tau_e$	**S=1**	**S=2**	**S=3**	**S=4**	**S=5**	**S=6**
1	**1**	110	010	011	001	101	100
1	**0**	111	000	111	000	111	000
1	**-1**	101	100	110	010	011	001
0	**1**	010	011	001	101	100	110
0	**0**	000	111	000	111	000	111
0	**-1**	001	101	100	110	010	011

Table 2. Faulty operation DTC switching table for configurations 1 and 3.

$d\lambda_s$	$d\tau_e$	**S=1**	**S=2**	**S=3**	**S=4**
1	**1**	10	11	01	00
1	**0**	00	10	11	01
0	**1**	11	01	00	10
0	**0**	01	00	10	11

Table 3. Faulty operation DTC switching table for configuration 2.

$d\lambda_s$	$d\tau_e$	**S=1**	**S=2**	**S=3**	**S=4**	**S=5**	**S=6**
1	**1**	101	100	110	010	011	001
1	**0**	111	000	111	000	111	000
1	**-1**	011	001	101	100	110	010
0	**1**	100	110	010	011	001	101
0	**0**	000	111	000	111	000	111
0	**-1**	010	011	001	101	100	110

Table 4. Induction motor parameters.

Parameter	Value
r_s	15.1 Ω
l_s	39.9 mH
r_r	6.22 Ω
l_r	39.9 mH
l_{ls}	523.8 mH
Number of poles pairs	1
Rated power	500 W

Figs. 3, 4 and 5 show phase currents and dq currents for configurations 1, 2 and 3, respectively, when DTC method is applied. For all configurations, a fault takes place in phase 1 at the time of 1.8 s. During 0.1 s the same switching table of healthy operation is maintained (see Table 1) and the triac is still turned-off, resulting in highly distorted currents in the remaining healthy phases. The interval between 1.8 s and 1.9 s is named "Faulty operation before compensation". At time 1.9 s, the compensation strategy is

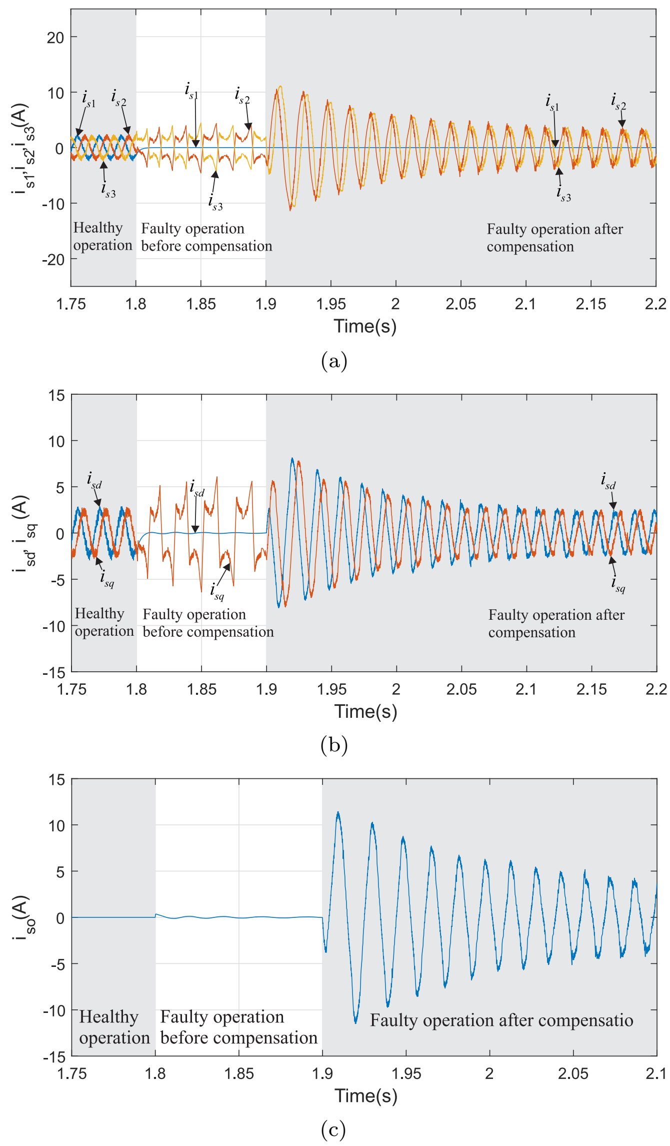

Figure 3. DTC - Configuration 1. (a) Phase currents. (b) dq currents. (c) i_{so}.

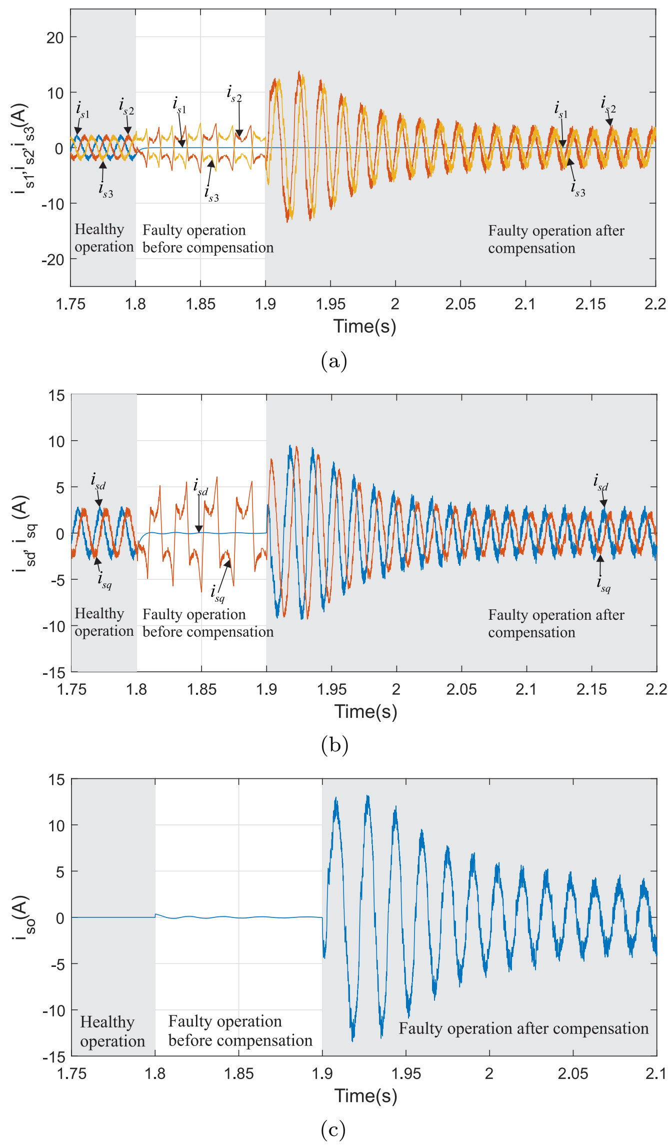

Figure 4. DTC - Configuration 2. (a) Phase currents. (b) dq currents. (c) i_{so}.

activated. i.e., triac is fired and switching states of Table 2 are applied for configurations 1 and 3 and of Table 3 for configuration 2. After 1.9 s, the system operates in the "Faulty operation after compensation".

After the fault, the power required from the motor is kept the same as before the fault. In this way, the compensation strategy intends to obtain the same dq currents as before the fault in order to maintain circular flux trajectory. As shown in Figs. 3(a) and 4(a) for configurations 1 and 2, respectively, after compensation currents in phases 2 and 3 (i_{s2} and i_{s3}) assume high amplitudes, since same power is kept as before the occurrence of the fault. It is worth noting that the motor and the inverter must be designed to cope with these currents or the system must operate in a derated condition due to thermal constraints. Due to the presence of zero-sequence current component, i_{s2} and i_{s3} become 60° out-of-phase. For configuration 3, on the other hand, phase currents assume practically same waveform and amplitude as before the fault (see Fig. 5(a)). Also, note that dq currents assume practically same waveform as before the fault for all configurations (see Figs. 3(b), 4(b) and 5(b) for configurations 1, 2 and 3, respectively).

Figs. 3(c), 4(c) and 5(c) are the zero-sequence currents i_{so} for configurations 1, 2 and 3, respectively. As mentioned before, these currents are null during healthy operation, but with the connection of neutral point to the dc-link mid-point (configuration 1) or a converter leg (configuration 2) they assume high values since they become part of the compensation strategy. On the other hand, for configuration 3, i_{so} is practically null during all the time, since the faulty phase is reconnected to the system (see Fig. 5(c)).

Figs. 6(a), 6(b) and 6(c) illustrate the flux trajectory in the "Faulty operation after compensation" for configurations 1, 2 and 3, respectively, when DTC method is applied. Note that the circular flux trajectory is maintained by means of the compensation strategy. In this way, it is possible to conclude that DTC is able to provide fault-tolerant operation in three-phase induction motor drives.

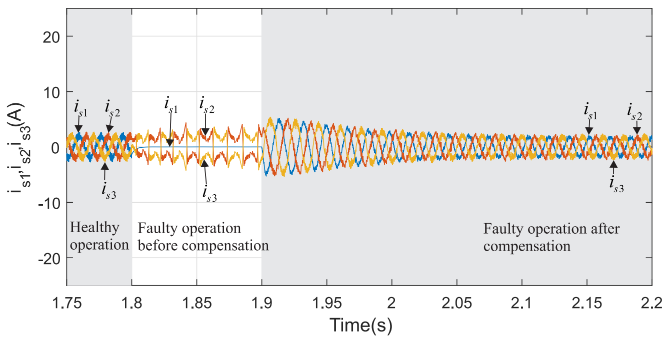

(a)

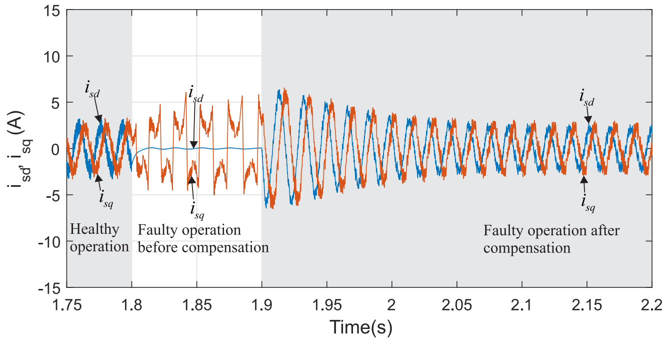

(b)

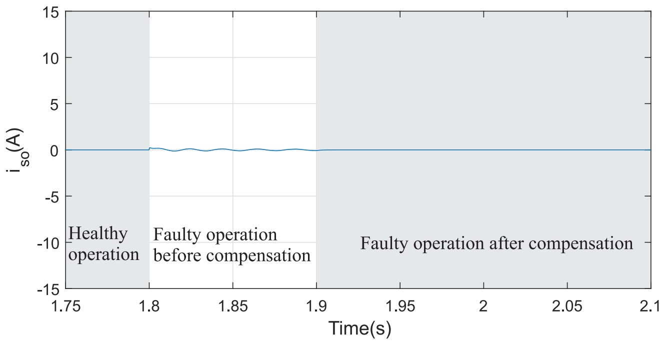

(c)

Figure 5. DTC - Configuration 3. (a) Phase currents. (b) dq currents. (c) i_{so}.

For comparison purposes, Figs. 7, 8, and 9 show phase currents and dq currents for configurations 1, 2, and 3, respectively, when FOC method is applied. The simulation results for FOC follow the same methodology as used previously for the DTC method. Note that DTC presents a smoother current transient-state than FOC, which provides high current oscillations. Furthermore, the new steady-state, after the fault, with the compensation strategy is reached in a shorter time with DTC.

Fig. 10 shows rotor speed and machine electromagnetic torque waveforms for all three configurations using both DTC and FOC for healthy and faulty operation modes. So, Figs. 10(a) and 10(b) illustrate these curves for configuration 1 for DTC and FOC, respectively. It is possible to see that, with DTC, the speed drops rapidly before the compensation takes place, but once this strategy is activated, the rotor speed value rapidly converges to the reference value. On the other hand, with FOC, rotor speed oscillates more and takes more time to converge to the reference value after the compensation strategy is activated.

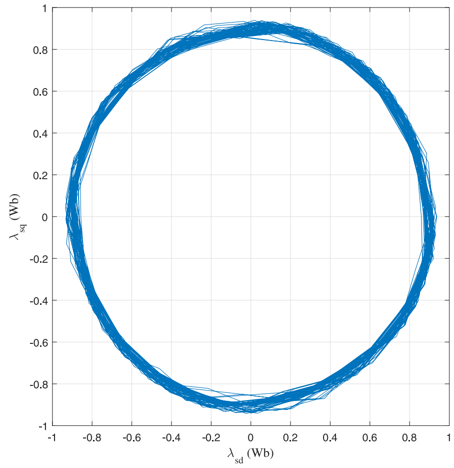

(a)

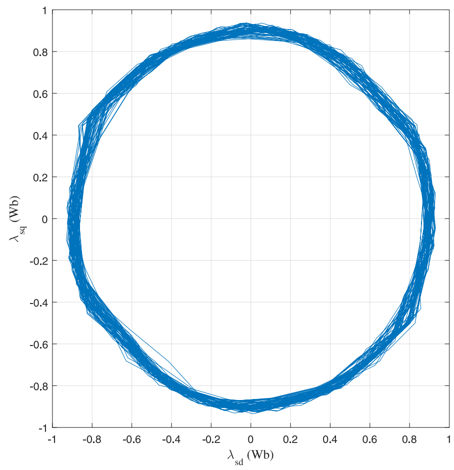

(b)

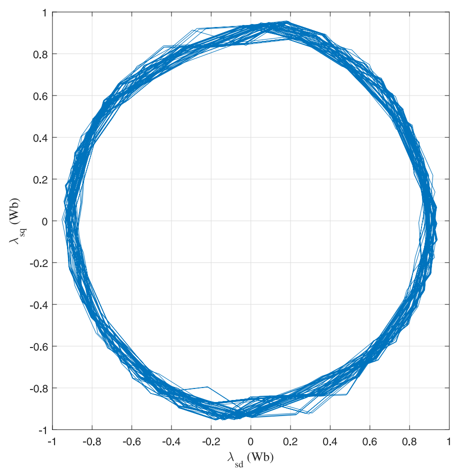

(c)

Figure 6. DTC - Stator flux trajectory with fault compensation. (a) Configuration 1. (b) Configuration 2. (c) Configuration 3.

Also, when the compensation strategy is employed, the use of FOC provides high torque ripple before steady-state is reached, which is not observed when DTC is applied. This shows, once again, that in fact the DTC method has better transient response than FOC. Similarly, Figs. 10(c) and 10(d) show the rotor speed and torque for configuration 2 for DTC and FOC, respectively, and Figs. 10(e) and

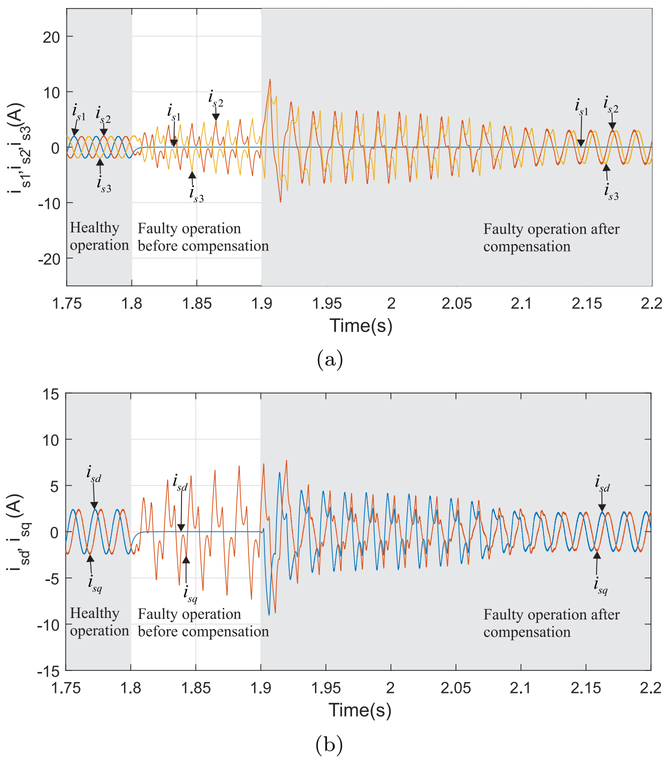

Figure 7. FOC - configuration 1. (a) Phase currents. (b) dq currents.

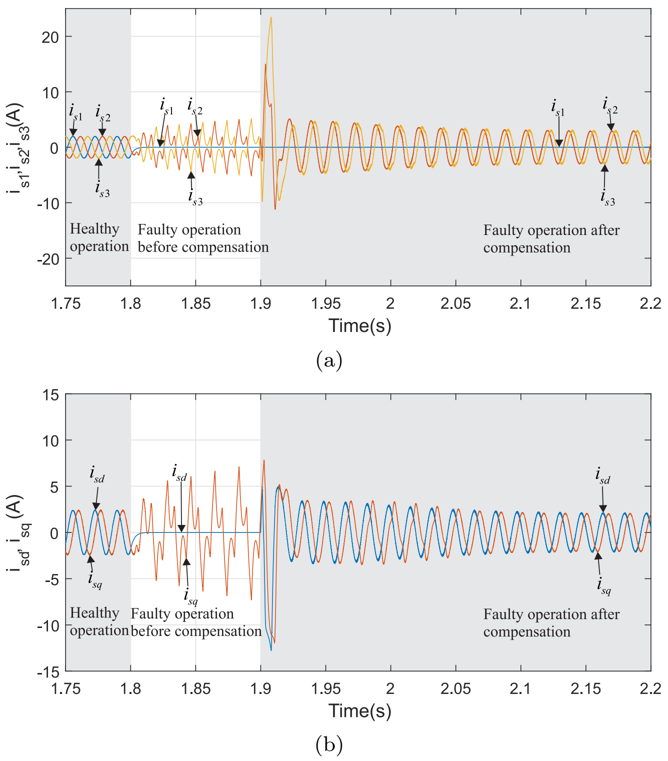

Figure 8. FOC - configuration 2. (a) Phase currents. (b) dq currents.

10(f) show the same waveforms for configuration 3. Same observations made for configuration 1 may be made for configurations 2 and 3 as well.

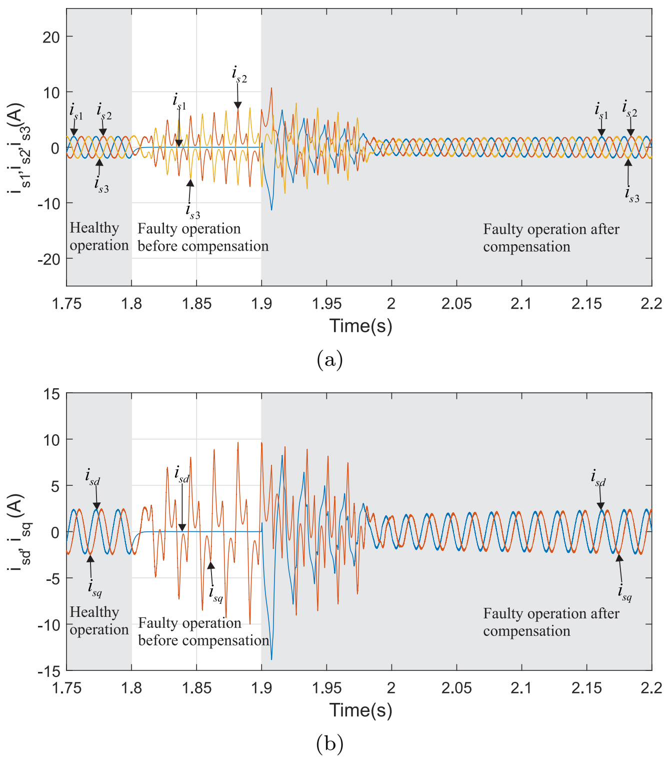

Figure 9. FOC - configuration 3. (a) Phase currents. (b) dq currents.

In this way, by comparing current, speed and torque responses, it is possible to confirm that DTC is able to provide fault-tolerant operation, with sinusoidal post-fault currents and circular flux trajectory for all three studied configurations. Also, all three present smoother and faster transient response to the fault compensation strategy when DTC is employed in comparison to FOC.

6. CONCLUSION

This paper discussed three fault-tolerant induction motor drive systems operating under a single-phase open-circuit fault. Despite these systems have been already discussed in the literature, the papers always use FOC- or Volts-Hertz-based fault compensation strategies. This paper, on the other hand, discussed DTC-based compensation strategies.The switching states $\alpha-\beta$ planes for healthy and faulty conditions were shown and explained. For that, new switching tables were elaborated in order to assure stator flux circular trajectory even after the fault. Performed simulations and comparisons with FOC show that DTC-based compensation strategies are feasible. Configurations 1 and 2, that make use of zero-sequence current component, present high value of currents in the remaining healthy phases and make them be 60° out-of-phase. The dynamic performance of DTC were compared to FOC for all three configurations in the occurrence of a open-circuit fault. Results show that DTC-based compensation strategies present smoother and faster transient response when compared to FOC-based ones.

REFERENCES

Abassi, M., Khlaief, A., Saadaoui, O., Chaari, A., and Boussak, M. (2017). Performance analysis of pmsm dtc

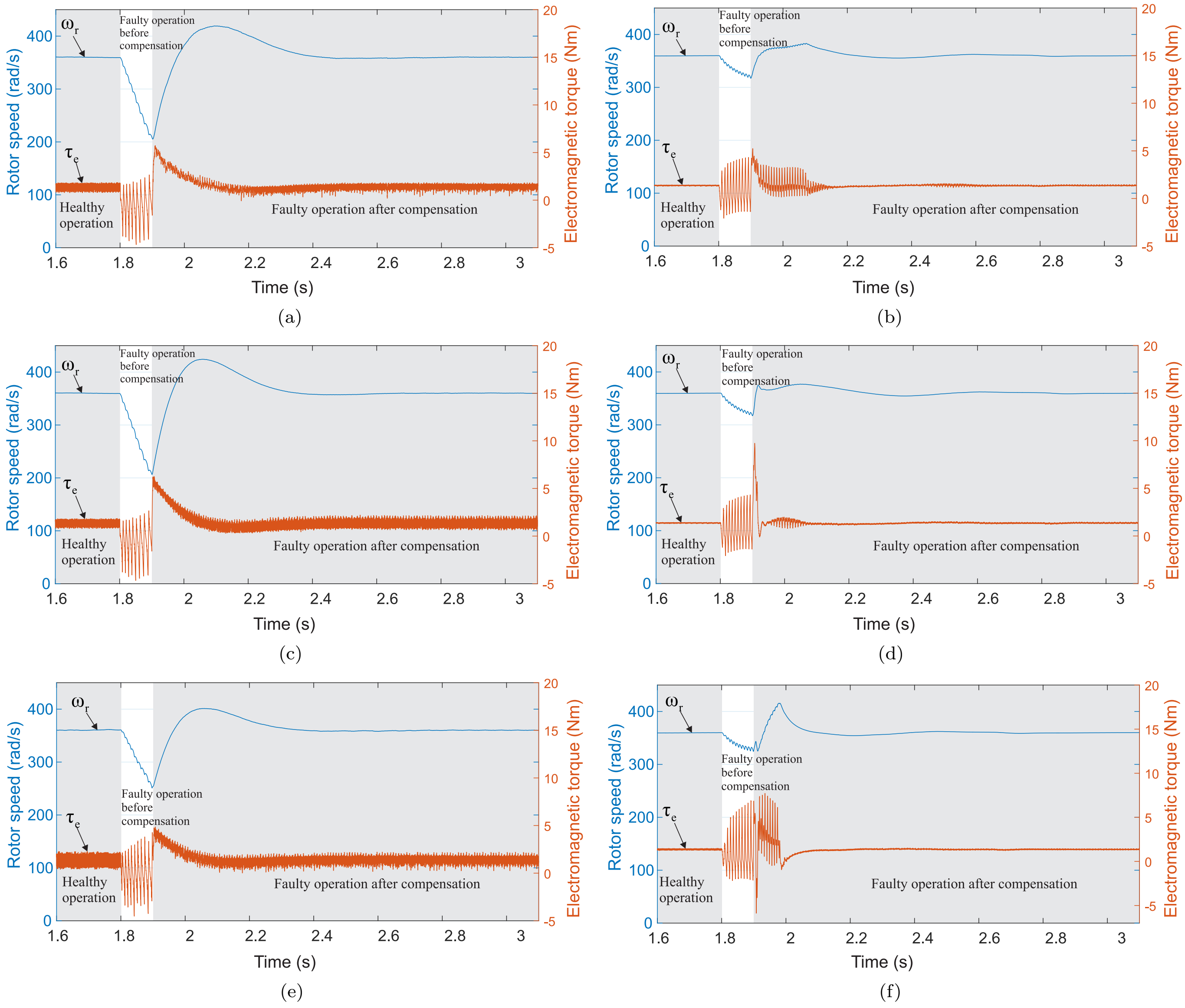

Figure 10. Rotor speed and electromagnetic torque. (a) DTC - Conf. 1. (b) FOC - Conf. 1. (c) DTC - Conf. 2. (d) FOC - Conf. 2. (e) DTC - Conf. 3. (f) FOC - Conf. 3.

drives under inverter fault. In *2017 International Conference on Advanced Systems and Electric Technologies (IC ASET)*, 244–249.

Beltrao de Rossiter Correa, M., Brandao Jacobina, C., Cabral da Silva, E.R., and Nogueira Lima, A.M. (2001). An induction motor drive system with improved fault tolerance. *IEEE Transactions on Industry Applications*, 37(3), 873–879.

Buja, G.S. and Kazmierkowski, M.P. (2004). Direct torque control of PWM inverter-fed AC motors - a survey. *IEEE Transactions on Industrial Electronics*, 51(4), 744–757.

Casadei, D., Profumo, F., Serra, G., and Tani, A. (2002). FOC and DTC: two viable schemes for induction motors torque control. *IEEE Transactions on Power Electronics*, 17(5), 779–787.

Dan Sun and Yikang He (2005). A modified direct torque control for pmsm under inverter fault. In *2005 International Conference on Electrical Machines and Systems*, volume 3, 2473 Vol. 3–2473.

de Araujo Ribeiro, R.L., Jacobina, C.B., da Silva, E.R.C., and Lima, A.M.N. (2004). Fault-tolerant voltage-fed pwm inverter ac motor drive systems. *IEEE Transactions on Industrial Electronics*, 51(2), 439–446.

Scarcella, G., Scelba, G., Pulvirenti, M., and Lorenz, R.D. (2017). Fault-tolerant capability of deadbeat-direct torque and flux control for three-phase pmsm drives. *IEEE Transactions on Industry Applications*, 53(6), 5496–5508.

Takahashi, I. and Noguchi, T. (1986). A new quick-response and high-efficiency control strategy of an induction motor. *IEEE Transactions on Industry Applications*, IA-22(5), 820–827.

Welchko, B.A., Lipo, T.A., Jahns, T.M., and Schulz, S.E. (2004). Fault tolerant three-phase ac motor drive topologies: a comparison of features, cost, and limitations. *IEEE Transactions on Power Electronics*, 19(4), 1108–1116.